Chapter 8

Results

This chapter discusses the results of the different fit configurations and hypothesis tests performed in the analysis. After the background estimation obtained through a background-only fit in the CRs is validated in the VRs, the SRs are unblinded and the observed data is compared to the SM background expectation.

8.1 Background-only fit results

8.1.1 Results in the control regions

As all CRs are mutually exclusive, a background-only fit simultaneously using information from all CRs can be run. Only the terms for the CRs enter the likelihood as channels and any signal contamination present in the CRs is neglected. This allows to fit the dominant backgrounds to data, and thus, by construction, leads to a good agreement between observed data and the total fitted background estimate in all CRs. The free normalisation parameters for $t\bar{t}$ (μ_{T}), single top (μ_{ST}) and $W + \text{jets}$ (μ_{W}) are fitted to be

$$
\begin{aligned}
\mu_{\text{T}} &= 1.02^{+0.07}_{-0.09}, \\
\mu_{\text{ST}} &= 0.6^{+0.5}_{-0.25}, \\
\mu_{\text{W}} &= 1.22^{+0.26}_{-0.24}.
\end{aligned}
\tag{8.1}
$$

While the dominant $t\bar{t}$ background stays roughly at its nominal expectation with respect to MC simulation, $W + \text{jets}$ processes are slightly scaled up, and the single top expectation is scaled down. The high uncertainty on μ_{ST} can be attributed to the relatively low MC statistics and comparably low purity of single top events in STR.

Table 8.1 summarises the background estimate including all uncertainties for all control regions after the fit. As discussed in chapter 6, $t\bar{t}$ dominates in all control regions except WR, where $W + \text{jets}$ is the largest background, followed by single top and $W + \text{jets}$ processes. Due to the relatively small normalisation factor for single top processes, $t\bar{t}$ and single top contribute to roughly equal amounts to STR. Small contributions come from diboson, multiboson as well as other backgrounds like $t\bar{t} + V$, $t\bar{t} + h$ and $V + h$. All processes estimated directly from MC
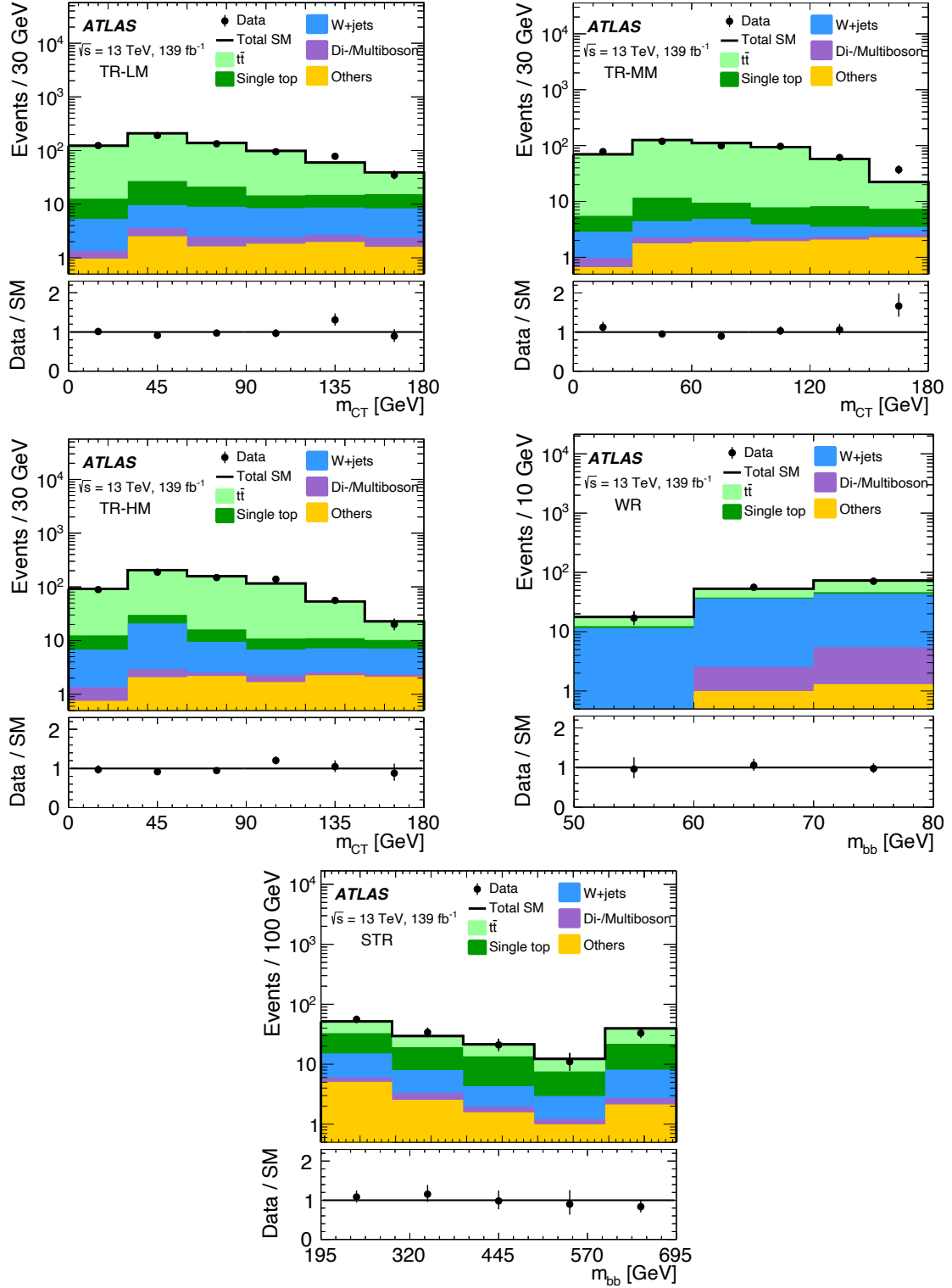
Figure 8.1: Exemplary distribution shown in each control region after the background-only fit. The shaded region includes all systematic uncertainties as well as MC statistical uncertainty. The $t\bar{t}$, single top and W + jets are normalised simultaneously in all CRs. A good agreement between MC expectation and data is observed in all CRs. Adapted from Ref. [170].

Table 8.1: Background-only fit results for the CRs for an integrated luminosity of $139\,\mathrm{fb}^{-1}$. Nominal MC expectations (normalised to MC cross-sections) are given for comparison. The errors shown include the MC statistical and systematic uncertainties. PDG rounding is applied to the event rates and uncertainties [7].

Region	TR-LM	TR-MM	TR-HM	WR	STCR
Observed events	657	491	641	144	155
Fitted SM events	666 ± 25	480 ± 21	645 ± 26	143 ± 12	154 ± 15
$t\bar{t}$	560 ± 40	430 ± 33	550 ± 40	47 ± 9	59 ± 12
Single top	60 ± 40	27 ± 23	33 ± 27	5 ± 4	57 ± 22
$W + \text{jets}$	34 ± 8	10.5 ± 2.8	44 ± 11	83 ± 16	23 ± 6
Di-/Multiboson	4.3 ± 1.2	2.0 ± 0.5	2.8 ± 0.5	5.7 ± 1.0	2.8 ± 0.9
Other	10.5 ± 1.3	10.6 ± 1.4	11.1 ± 1.4	2.4 ± 0.4	12.3 ± 1.5
MC exp. SM events	720 ± 80	474 ± 33	680 ± 50	130 ± 13	180 ± 50
$t\bar{t}$	570 ± 70	407 ± 30	570 ± 40	46 ± 10	52 ± 10
Single top	102 ± 18	46 ± 13	58 ± 16	9 ± 6	90 ± 40
$W + \text{jets}$	29 ± 4	8.4 ± 1.2	36.1 ± 3.1	67 ± 5	19.0 ± 2.0
Di-/Multiboson	4.1 ± 1.1	2.0 ± 0.5	2.8 ± 0.5	5.6 ± 1.0	2.8 ± 0.9
Other	10.6 ± 1.3	10.6 ± 1.4	11.2 ± 1.4	2.5 ± 0.4	12.4 ± 1.5

simulation cumulatively account for only 10%, 5.5% and a maximum of 2.6% in the single top, $W + \text{jets}$ and $t\bar{t}$ control regions, respectively. Exemplary distributions in the CRs after the background-only fit are shown in fig. 8.1, revealing a good agreement between observed data and the SM background estimate throughout the distributions shown.

8.1.2 Results in the validation regions

In order to validate the extrapolations from the CRs to the SRs, the results of the background-only fit in the CRs are extrapolated into the VRs. Table 8.2 summarises the observed data and SM background estimate in the different VR bins before and after the background-only fit in the CRs. Exemplary $N-1$ distributions in m_{CT} in all VRs are shown in fig. 8.2.

In the on-peak VRs, designed to validate the extrapolation from the control regions over the $m_{b\bar{b}}$ distribution, $t\bar{t}$ is by far the dominant background after the background-only fit. Contributions from single top and $W + \text{jets}$ each amount to only 1–5%, depending on the validation region bin. Diboson, multiboson and other SM processes result in minor contributions of the level of not more than 3% of the total background estimate. As the total uncertainties on the background estimate in the on-peak regions are dominated by the $t\bar{t}$ uncertainties, the sizeable uncertainties on the $W + \text{jets}$ and single top estimates due to relatively limited MC statistics do not have a significant impact.

In the off-peak VRs, after the background-only fit, $t\bar{t}$ is the dominant process in the low mass regime, where contributions from single top and $W + \text{jets}$ are subdominant. In the medium and high mass regimes, $t\bar{t}$, single top and $W + \text{jets}$ all result in similar contributions. Diboson, multiboson and other SM processes are only minor backgrounds in all off-peak regions,
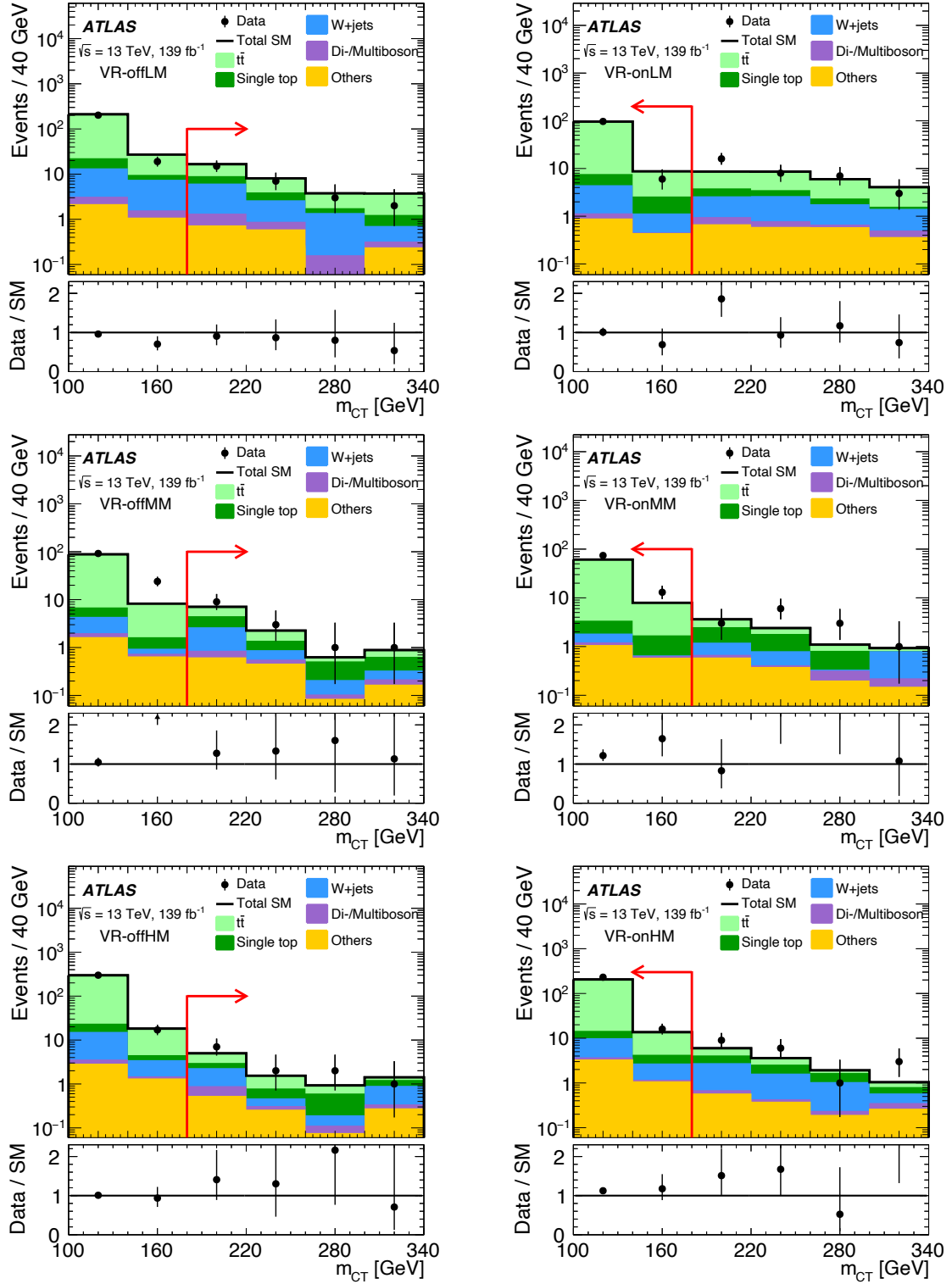
Figure 8.2: Exemplary $N-1$ distributions shown in each validation region after the background-only fit with subsequent extrapolation to the VRs. All selection cuts except for the requirement on m_{CT} (indicated using the red arrow) are applied. The shaded region includes all systematic uncertainties as well as MC statistical uncertainty. Adapted from Ref. [170].

Table 8.2: Background-only fit results from the CRs extrapolated to the VRs for an integrated luminosity of 139 fb^{-1}. Nominal MC expectations (normalised to MC cross-sections) are given for comparison. The errors shown include the MC statistical and systematic uncertainties. Uncertainties in the fitted event rates are symmetric by construction, except where the negative error is truncated at an event rate of zero. PDG rounding is applied to the event rates and uncertainties [7].

Region	VR-onLM	VR-onMM	VR-onHM	VR-offLM	VR-offMM	VR-offHM
Observed events	103	87	247	27	14	12
Fitted SM events	100 ± 19	64 ± 9	215 ± 18	34 ± 6	9.5 ± 2.7	7.5 ± 2.6
$t\bar{t}$	90 ± 19	59 ± 9	196 ± 19	18 ± 4	2.4 ± 1.4	1.8 ± 1.8
Single top	5^{+5}_{-5}	$2.6^{+2.9}_{-2.6}$	6 ± 6	5 ± 4	3.0 ± 1.8	1.8 ± 1.5
$W + \text{jets}$	4 ± 4	0.6 ± 0.5	7.9 ± 2.1	8.2 ± 2.6	2.3 ± 0.8	2.2 ± 0.6
Di-/Multiboson	0.24 ± 0.08	0.19 ± 0.08	0.54 ± 0.19	1.07 ± 0.27	0.39 ± 0.11	0.51 ± 0.14
Other	1.34 ± 0.22	1.67 ± 0.28	4.4 ± 2.0	1.6 ± 0.5	1.34 ± 0.25	1.15 ± 0.24
MC exp. SM events	110 ± 40	69 ± 17	218 ± 22	34 ± 7	12.8 ± 3.4	9.7 ± 3.3
$t\bar{t}$	92 ± 35	62 ± 17	196 ± 21	16 ± 5	3.8 ± 2.2	3.1 ± 1.9
Single top	8 ± 5	4.5 ± 3.4	11 ± 6	9 ± 4	5.3 ± 2.2	3.1 ± 2.5
$W + \text{jets}$	2.8 ± 2.3	0.5 ± 0.5	6.5 ± 1.2	6.5 ± 1.6	2.0 ± 0.5	1.80 ± 0.34
Di-/Multiboson	0.24 ± 0.07	0.19 ± 0.08	0.50 ± 0.17	1.07 ± 0.28	0.37 ± 0.10	0.50 ± 0.15
Other	1.35 ± 0.23	1.70 ± 0.28	4.4 ± 0.9	1.6 ± 0.5	1.36 ± 0.25	1.16 ± 0.24

cumulatively amounting to only 10–14% of the total background estimate, depending on the mass regime.

The agreement between data and the background estimate is summarised in fig. 8.4. In VR-onMM and and VR-onHM, light overfluctuations of 1.3σ and 1.7σ, respectively, are observed in data. In the remaining VRs, the agreement between observed data and SM expectation is within 1σ. The overall agreement in the validation regions is thus considered to be acceptable, paving the way for further extrapolation of the background estimate into the SRs.

8.1.3 Results in the signal regions

By extrapolating the results from the background-only fit in the control regions, the background estimate in the signal regions can be obtained. In the following, the results in all discovery and exclusion signal regions are discussed.

Table 8.3 compares the background estimate with the observed data for all discovery signal regions. In the low-mass discovery signal region, $t\bar{t}$ is the dominant background, followed by $W + \text{jets}$ and single top. At higher values of m_{T}, in the medium-mass discovery signal region, all three main SM backgrounds contribute to roughly equal amounts. Finally, in the high-mass signal region, $W + \text{jets}$ is the largest SM background, followed by single top and $t\bar{t}$. In all discovery signal regions, diboson, multiboson and other SM backgrounds yield only minor contributions. The results in the exclusion signal regions are shown in table 8.4. As for the discovery signal regions, $t\bar{t}$ is the dominant background in the low-mass exclusion signal region bins SR-LM, while $W + \text{jets}$ slightly dominates in the high-mass exclusion signal region bins SR-HM. The m_{CT} distributions of all three exclusion SRs are shown in fig. 8.3.

Table 8.3: Background-only fit results extrapolated to the discovery SRs for an integrated luminosity of $139\,\mathrm{fb}^{-1}$. Nominal MC expectations (normalised to MC cross-sections) are given for comparison. The errors shown include the MC statistical and systematic uncertainties. Uncertainties in the fitted yields are symmetric by construction, except where the negative error is truncated at an event yield of zero. PDG rounding is applied to the event rates and uncertainties [7].

Region	SR-LM (disc.)	SR-MM (disc.)	SR-HM (disc.)
Observed events	66	32	14
Fitted SM events	47 ± 6	21 ± 5	8.6 ± 2.8
$t\bar{t}$	22 ± 4	5.9 ± 1.9	1.9 ± 0.7
Single top	9 ± 6	6 ± 5	$2.0^{+2.4}_{-2.0}$
$W + \mathrm{jets}$	11.1 ± 2.9	5.6 ± 1.4	3.7 ± 1.0
Di-/Multiboson	1.23 ± 0.24	0.56 ± 0.11	0.21 ± 0.06
Other	4.8 ± 0.5	2.6 ± 0.4	0.74 ± 0.16
MC exp. SM events	50 ± 7	22 ± 5	8 ± 4
$t\bar{t}$	21 ± 5	4.9 ± 1.6	1.2 ± 0.6
Single top	14 ± 4	9 ± 5	$2.9^{+3.5}_{-2.9}$
$W + \mathrm{jets}$	9.1 ± 1.3	4.5 ± 0.7	3.0 ± 0.6
Di-/Multiboson	1.20 ± 0.23	0.56 ± 0.11	0.21 ± 0.06
Other	4.8 ± 0.5	2.6 ± 0.4	0.74 ± 0.16

None of the exclusion or discovery signal regions reveal a significant deviation in data compared to the SM expectation, and all observations are in good agreement with the SM. A slight overfluctuation of data in the discovery SRs is quantified to be within 1.8σ, 1.6σ and 1.2σ in the discovery signal regions SR-LM, SR-MM and SR-HM, respectively[†]. In the exclusion signal regions, the agreement between data and SM expectation is well within 1σ, except for the SR-LM low m_{CT}, SR-MM medium m_{CT} and SR-HM high m_{CT} bins, where a slight overfluctuation of 1.5σ, 1.6σ and 1.3σ, respectively, is observed in data. Figure 8.4 summarises across all regions the observed data, SM background expectation as well as the significances of any deviations.

Since no significant excess is seen in data, the signal regions will be used in the following to derive model-dependent exclusion limits as well as model-independent upper limits on the visible cross section. As a consequence of the minor overfluctuations of data observed in some signal region bins, the observed model-dependent and model-independent limits will be slightly weaker than expected.

[†] The discovery signal regions are not mutually exclusive, thus the small overfluctuations observed in data are not statistically independent in these regions.

Table 8.4: Background-only fit results in the exclusion SRs for an integrated luminosity of $139\,\mathrm{fb}^{-1}$. The first column shows the sum of all m_{CT} bins (including overflow). Subsequent columns indicate the different bins in m_{CT}, overflow is included in the last bin. The errors shown include the MC statistical and systematic uncertainties. Uncertainties in the fitted yields are symmetric by construction, except where the negative error is truncated at an event yield of zero. PDG rounding is applied to the event rates and uncertainties [7]. Table adapted from [170].

| **SR-LM**	All m_{CT} bins	Low m_{CT}	Medium m_{CT}	High m_{CT}
Observed	34	16	11	7
Expected	27 ± 4	8.8 ± 2.8	11.3 ± 3.1	7.3 ± 1.5
$t\bar{t}$	16.2 ± 3.4	4.4 ± 2.2	7.3 ± 2.5	4.6 ± 1.2
Single top	2.7 ± 1.8	1.3 ± 1.1	$0.9^{+1.0}_{-0.9}$	0.6 ± 0.6
W+jets	5.5 ± 2.0	2.0 ± 0.9	2.4 ± 1.3	1.1 ± 0.5
Di-/Multiboson	0.67 ± 0.19	0.39 ± 0.13	$0.09^{+0.11}_{-0.09}$	0.18 ± 0.04
Others	2.23 ± 0.29	0.81 ± 0.25	0.64 ± 0.15	0.77 ± 0.12
SR-MM	All m_{CT} bins	Low m_{CT}	Medium m_{CT}	High m_{CT}
Observed	13	4	7	2
Expected	8.6 ± 2.2	4.6 ± 1.7	2.6 ± 1.3	1.4 ± 0.6
$t\bar{t}$	2.7 ± 1.4	1.6 ± 0.9	0.8 ± 0.7	0.30 ± 0.24
Single top	2.7 ± 1.9	1.6 ± 1.5	$1.0^{+1.1}_{-1.0}$	$0.15^{+0.19}_{-0.15}$
W+jets	1.5 ± 0.7	0.6 ± 0.4	$0.3^{+0.4}_{-0.3}$	0.57 ± 0.26
Di-/Multiboson	0.29 ± 0.08	0.09 ± 0.04	0.065 ± 0.028	0.14 ± 0.06
Others	1.33 ± 0.27	0.69 ± 0.20	0.40 ± 0.13	0.24 ± 0.09
SR-HM	All m_{CT} bins	Low m_{CT}	Medium m_{CT}	High m_{CT}
Observed	14	6	5	3
Expected	8.1 ± 2.7	4.1 ± 1.9	2.9 ± 1.3	1.1 ± 0.5
$t\bar{t}$	1.4 ± 0.5	0.8 ± 0.4	0.36 ± 0.25	0.22 ± 0.15
Single top	$2.0^{+2.4}_{-2.0}$	$0.9^{+1.5}_{-0.9}$	0.9 ± 0.9	$0.16^{+0.26}_{-0.16}$
W+jets	3.7 ± 1.0	1.9 ± 0.8	1.4 ± 0.8	0.45 ± 0.19
Di-/Multiboson	0.21 ± 0.06	0.057 ± 0.025	0.075 ± 0.027	0.08 ± 0.04
Others	0.74 ± 0.16	0.34 ± 0.09	0.19 ± 0.08	0.21 ± 0.08
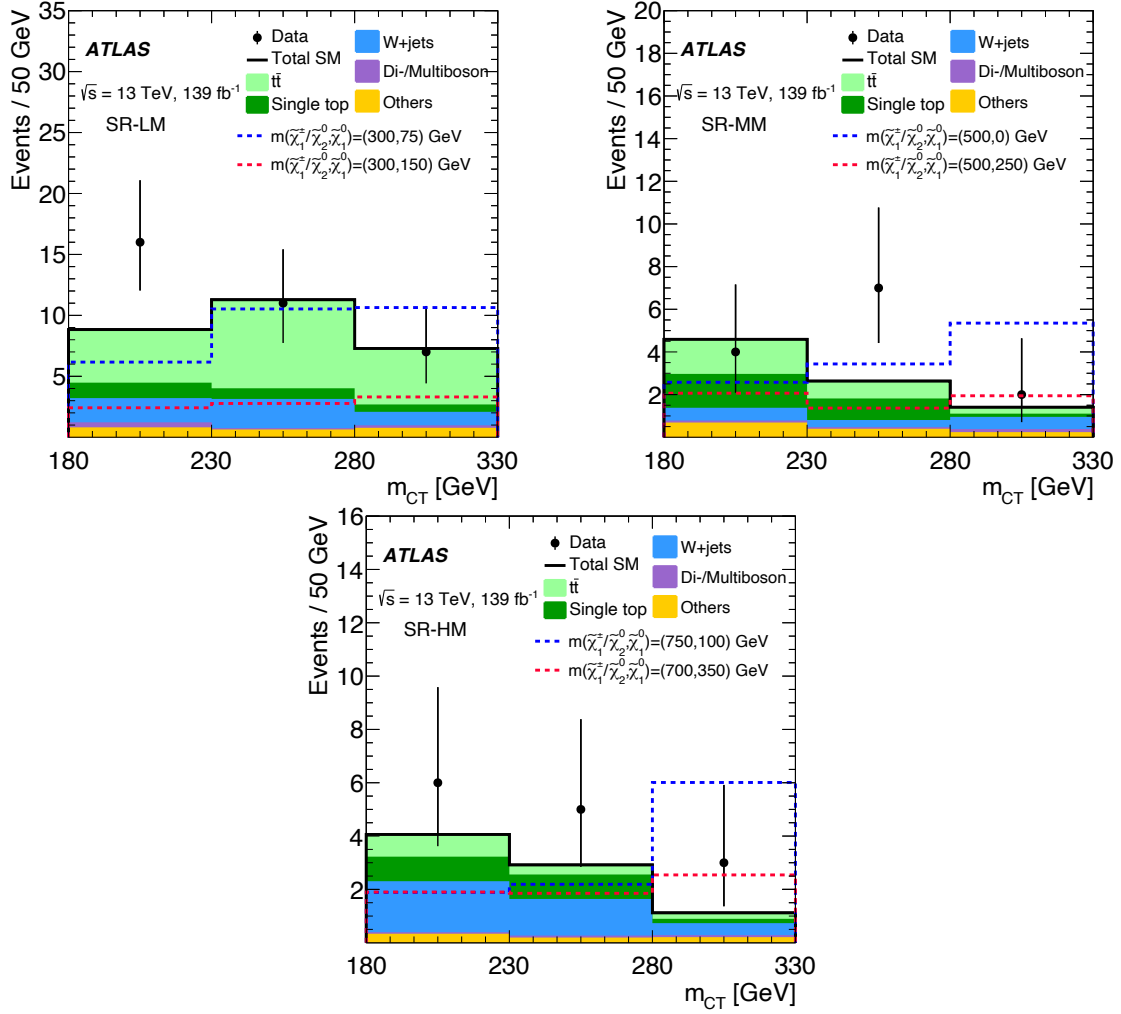
Figure 8.3: Exemplary distribution shown in each exclusion signal region after the background-only fit. The shaded region includes all systematic uncertainties (including correlations) as well as MC statistical uncertainty. Adapted from Ref. [170].
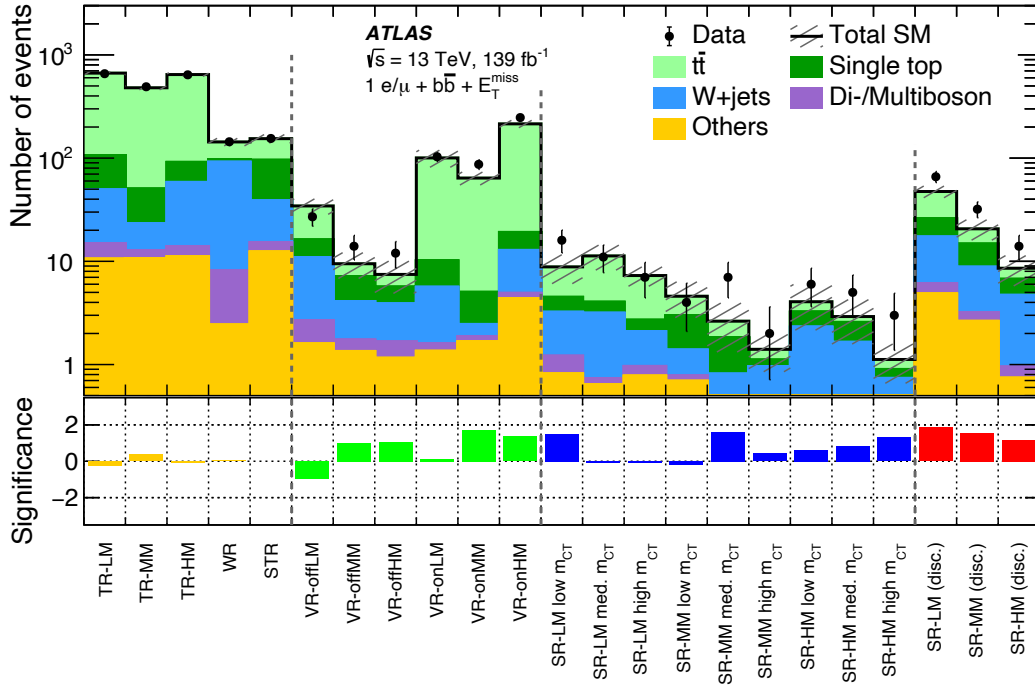
Figure 8.4: Comparison of the observed data and expected event rates in all regions considered in the analysis. The shaded uncertainty band includes both MC statistical and systematic uncertainties. The significances [165] of the differences between the observed data and expected event rates are shown in the bottom panel. The discovery signal regions are not statistically independent from each other, nor from the exclusion signal regions. Figure adapted from Ref. [170].

8.2 Interpretation

As no significant excess of data is observed in any of the signal regions, model-independent upper limits as well as model-dependent exclusion limits are computed.

8.2.1 Model-independent upper limits

Model-independent upper limits on the visible cross section of BSM processes are derived using the discovery signal regions. For this, a likelihood containing terms for the control regions and the discovery signal regions is used. Since the discovery signal regions are not statistically independent from each other, only one region enters the likelihood at a time. This results in three distinct fit configurations in which the signal strength μ is the POI and no signal contamination is assumed in the control regions. The POI is subsequently scanned in distinct steps from zero to high values[†], followed by a hypothesis test at each scan step. The upper limit on the number of observed signal events S_{obs}^{95} is then given by the value of μ for which the corresponding CL_s value drops below 0.05. An upper limit on the visible cross section $\langle\epsilon\sigma\rangle_{\text{obs}}^{95}$ is obtained by dividing S_{obs}^{95} by the integrated luminosity of $139\,\text{fb}^{-1}$. In addition to the upper limits on $\langle\epsilon\sigma\rangle_{\text{obs}}^{95}$ and S_{obs}^{95}, table 8.5 also gives the p-values (and corresponding significances) for rejecting the background-only hypothesis in favour of the signal-plus-background hypothesis. As all significances are well below 2σ for all SRs, the background-only hypothesis cannot be rejected.

8.2.2 Model-dependent exclusion limits

For each signal point in the signal grid considered, a separate *exclusion* fit is run using all control regions and exclusion signal regions. As all exclusion signal region bins are mutually exclusive, a likelihood containing terms for all nine signal region bins can be constructed, effectively creating a shape-fit in the binned variables m_{T} and m_{CT} (cf. chapter 5). As opposed to the background-only fit, the exclusion fits allow for signal contribution in all regions considered. For each point in the signal grid, the expected and observed CL_s value is calculated as discussed in section 3.4. Expected (observed) contour lines can then be drawn at expected (observed) $\text{CL}_s = 0.05$ in the $m(\tilde{\chi}_1^{\pm}/\tilde{\chi}_2^0)$–$m(\tilde{\chi}_1^0)$ space spanned by the simplified model parameters. Signal

---

[†] The signal strength is in principle allowed to exceed unity in order for the scan to find a 95% CL upper limit

Table 8.5: The 95% CL upper limits on the visible cross-section ($\langle\epsilon\sigma\rangle_{\text{obs}}^{95}$) and on the number of signal events (S_{obs}^{95}) are given. Additionally, the expected 95% CL upper limits on the number of signal events if no BSM signal is present (S_{exp}^{95}) are given, including their $\pm1\sigma$ excursions. The last three columns indicate the confidence level observed for the background-only hypothesis (CL_{B}), the discovery p-value (p_0) and the significance Z [165].

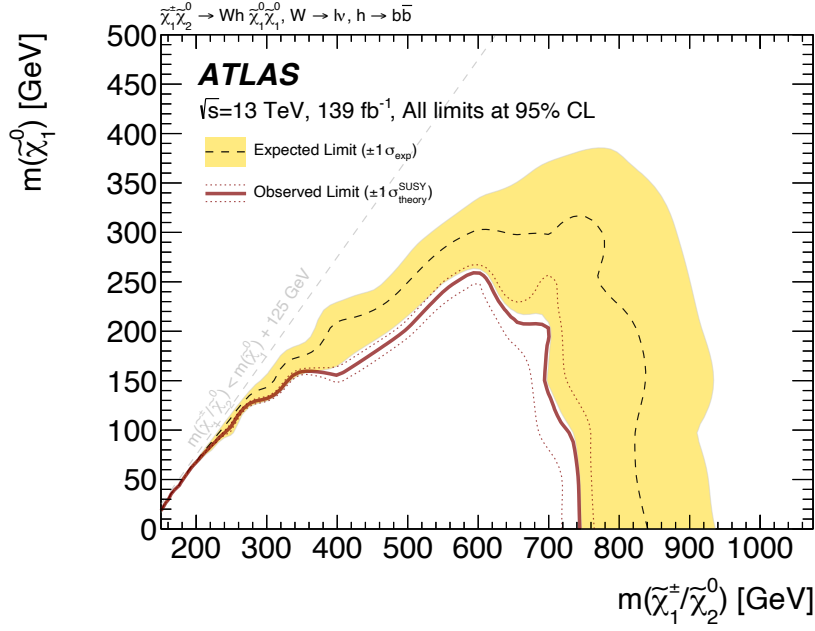| Signal Region	$\langle\epsilon\sigma\rangle_{\text{obs}}^{95}$[fb]	S_{obs}^{95}	S_{exp}^{95}	CL_{B}	p_0	Z
SR-LM (disc.)	0.26	36.8	$20.0^{+8.0}_{-5.4}$	0.97	0.03	1.88
SR-MM (disc.)	0.18	24.8	$15.3^{+6.2}_{-4.6}$	0.94	0.06	1.54
SR-HM (disc.)	0.11	14.7	$9.7^{+3.3}_{-2.7}$	0.89	0.10	1.30

Figure 8.5: Model-dependent exclusion contour on $\tilde{\chi}_1^\pm/\tilde{\chi}_2^0$ pair production. The dashed black line represents the expected limit obtained using Asimov data. The uncertainties are given by the yellow band. The red solid line represents the observed limit obtained using $139\,\mathrm{fb}^{-1}$ of data taken by ATLAS. By varying the signal cross sections up and down by their uncertainty, the red dashed lines are obtained. All contours are given at 95% CL. Figure adapted from Ref. [170].

points inside the contour are then excluded at 95% CL. Figure 8.5 shows the exclusion contours obtained in the signal grid considered for the $\tilde{\chi}_1^\pm\tilde{\chi}_2^0$ simplified mdoel in the 1ℓ search. The dashed line corresponds to the expected exclusion contour, obtained using the Asimov dataset. The yellow uncertainty band represents the interval containing 68% of all exclusion contours obtained for repeated observations distributed according to the background-only hypothesis. The solid red line represents the observed exclusion limit obtained using the data recorded by ATLAS. As discussed in section 7.2.2, the dashed red lines are obtained by varying the signal cross sections up and down by 1σ.

Due to the slight overfluctuations of data observed in some of the exclusion signal region bins, the observed limit is slightly weaker than the expected one. The observed exclusion limit extends to about $740\,\mathrm{GeV}$ in $m(\tilde{\chi}_1^\pm/\tilde{\chi}_2^0)$ for models with a massless $\tilde{\chi}_1^0$, and up to $600\,\mathrm{GeV}$ for models with $m(\tilde{\chi}_1^0) = 250\,\mathrm{GeV}$. This extends the previous limit set by ATLAS in this simplified model and decay channel by more than $200\,\mathrm{GeV}$ in $m(\tilde{\chi}_1^\pm/\tilde{\chi}_2^0)$ for a light $\tilde{\chi}_1^0$, an improvement made possible not only by the significant increase in integrated luminosity but also the introduction of a two-dimensional shape fit in the analysis strategy.

8.3 Discussion

At the time of writing, the limits derived in this analysis are the most stringent limits on the $\tilde{\chi}_1^\pm\tilde{\chi}_2^0 \rightarrow Wh\tilde{\chi}_1^0\tilde{\chi}_1^0$ simplified model set by an ATLAS search [244], surpassing not only
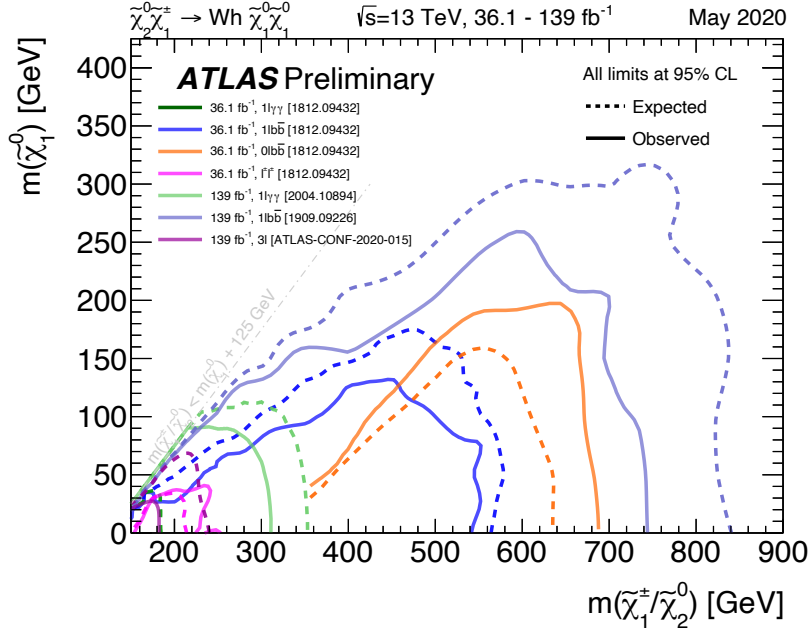
Figure 8.6: Summary of ATLAS limits on $\tilde{\chi}_1^\pm/\tilde{\chi}_2^0$ masses in the $\tilde{\chi}_1^\pm\tilde{\chi}_2^0 \to Wh\tilde{\chi}_1^0\tilde{\chi}_1^0$ simplified model. The exclusion limit obtained by the analysis presented in this work is referred to as *1Lbb* (the 139 fb^{-1} iteration) and is the most stringent limit in this simplified model set by an ATLAS search thus far. Figure adapted from Ref. [244].

the previous iteration of the analysis [168], but also yielding more stringent limits than those published by ATLAS in other decay channels of the same simplified model. Figure 8.6 shows a summary of results published by ATLAS searches in the $\tilde{\chi}_1^\pm\tilde{\chi}_2^0 \to Wh\tilde{\chi}_1^0\tilde{\chi}_1^0$ simplified model, the search presented in this thesis is referred to therein as '*1Lbb*'. Additional searches in the 0ℓ as well as 1ℓ final states are being worked on, and are expected to extend the limits[†] on $m(\tilde{\chi}_1^\pm/\tilde{\chi}_2^0)$ up to roughly 1 TeV for massless $\tilde{\chi}_1^0$ as well as slightly extend the excluded parameter space towards the diagonal where $m(\tilde{\chi}_1^\pm/\tilde{\chi}_2^0) = m(\tilde{\chi}_1^0) + m(h)$.

Various other searches for SUSY at both ATLAS and CMS are constraining a multitude of other supersymmetric particle production and decay processes. The limits on gluino and squark pair production at the LHC are particularly heavily constrained, reaching 2 TeV in many cases. With the large integrated luminosity available through the full Run 2 dataset and the improved analysis techniques and strategies developed over the last years, the typically weaker limits on electroweakinos and sleptons are also significantly increasing and in some cases approach the 1 TeV mark. The diverse SUSY search programs at ATLAS and CMS thus increasingly constrain the existence of SUSY at the TeV scale at the LHC. Still, a number of arguments can be made that discarding the possibility for SUSY to exist at the energies available with the LHC is much too early. By the end of the lifetime of the LHC (including the high luminosity upgrade HL-LHC), a projected amount of 3000 fb^{-1} [245] will have been delivered to the particle physics experiments. Many supersymmetric models not accessible with the full Run 2 dataset using today's analyses will hence only come into reach in the upcoming runs of the LHC.

[†]   Assuming that no significant excess in data is seen in the search regions of these analyses.

More importantly however, most of the quoted limits assume simplified models and are thus only valid if the assumptions of the respective simplified model are realised in nature. In any realistic supersymmetric scenario that might be realised in nature and is accessible to the LHC, assumptions like 100% branching fractions or a small set of supersymmetric particles participating in the decay chains are most likely not exactly fulfilled. Thus, the quoted simplified model limits can in general not be trivially interpreted as the true underlying constraint on the respective parameter of a more realistic supersymmetric scenario. Due to the optimistic assumptions like 100% branching fractions, the true constraints will in general be significantly weaker than the simplified model limits. Reinterpretations of Run 1 ATLAS searches for SUSY in the pMSSM [76] have indeed shown that constraints on the supersymmetric masses are somewhat weaker in more complex SUSY models, than those quoted for the simplified models studied in the respective analyses.

Naturally, there is a large interest in the HEP community—both within ATLAS as well as outside of the collaboration—to perform reinterpretations of the existing ATLAS searches for SUSY in new, promising signal models. Compelling reasons for performing reinterpretations include, amongst others, the possibility to state a combined sensitivity of the ATLAS SUSY search program to more realistic and complex SUSY scenarios (compared to the simplified model limits). However, especially when considering high-dimensional parameter spaces like the pMSSM, such reinterpretation quickly become computationally expensive and require appropriate approximations. For this reason, the next part of this thesis will introduce and discuss some of these approximations and show preliminary results of a reinterpretation of the 1ℓ search in the pMSSM.